Metabolic heterogeneity in human lung tumors

Christopher T. Hensley[1], **Brandon Faubert**[1], **Qing Yuan**[2], **Naama Lev-Cohain**[11], **Eunsook Jin**[3,4], **Jiyeon Kim**[1], **Lei Jiang**[1], **Bookyung Ko**[1], **Rachael Skelton**[5], **Laurin Loudat**[5], **Michelle Wodzak**[12], **Claire Klimko**[1], **Elizabeth McMillan**[6], **Yasmeen Butt**[7], **Min Ni**[1], **Dwight Oliver**[7], **Jose Torrealba**[7], **Craig R. Malloy**[2,3,4], **Kemp Kernstine**[8], **Robert E. Lenkinski**[2,3], and **Ralph J. DeBerardinis**[1,9,10,*]

[1]Children's Medical Center Research Institute, The University of Texas Southwestern Medical Center, Dallas, TX 75390, USA

[2]Department of Radiology, The University of Texas Southwestern Medical Center, Dallas, TX 75390, USA

[3]Advanced Imaging Research Center, The University of Texas Southwestern Medical Center, Dallas, TX 75390, USA

[4]Department of Internal Medicine, The University of Texas Southwestern Medical Center, Dallas, TX 75390, USA

[5]Clinical Research Office, The University of Texas Southwestern Medical Center, Dallas, TX 75390, USA

[6]Department of Cell Biology, The University of Texas Southwestern Medical Center, Dallas, TX 75390, USA

[7]Department of Pathology, The University of Texas Southwestern Medical Center, Dallas, TX 75390, USA

[8]Department of Cardiovascular and Thoracic Surgery, The University of Texas Southwestern Medical Center, Dallas, TX 75390, USA

[9]Department of Pediatrics, The University of Texas Southwestern Medical Center, Dallas, TX 75390, USA

[10]Eugene McDermott Center for Human Growth and Development, The University of Texas Southwestern Medical Center, Dallas, TX 75390, USA

[*]Contact: Ralph.deberardinis@utsouthwestern.edu, 5323 Harry Hines Blvd, Room NL12.138B, Dallas, TX 75390-8502. Tel: 214-648-2587. Fax: 214-648-5515.

[11]Hadassah Medical Center, Jerusalem, Israel

[12]Office of Animal Welfare Assurance, University of Oklahoma Health Sciences Center, Oklahoma City, OK 73104, USA

SUMMARY

Non-small cell lung cancer (NSCLC) is heterogeneous in the genetic and environmental parameters that influence cell metabolism in culture. Here, we assessed the impact of these factors on human NSCLC metabolism *in vivo* using intra-operative ^{13}C-glucose infusions in nine NSCLC patients to compare metabolism between tumors and benign lung. While enhanced glycolysis and glucose oxidation were common among these tumors, we observed evidence for oxidation of multiple nutrients in each of them, including lactate as a potential carbon source. Moreover, metabolically heterogeneous regions were identified within and between tumors, and surprisingly, our data suggested potential contributions of non-glucose nutrients in well-perfused tumor areas. Our findings not only demonstrate the heterogeneity in tumor metabolism *in vivo* but also highlight the strong influence of the microenvironment on this feature.

INTRODUCTION

Tumors display altered metabolism relative to benign tissues (Hanahan and Weinberg, 2011). These changes support abnormal survival and growth of malignant cells by providing energy, macromolecular precursors and reducing equivalents (DeBerardinis et al., 2008). Beyond the importance of metabolic reprogramming to cancer biology, it also has implications for clinical oncology. Targeting key metabolic activities is an effective therapeutic approach (Vander Heiden, 2011), and the ability to image informative aspects of metabolism has made it possible to identify and characterize malignant tissue non-invasively. The most widely used form of metabolic imaging is ^{18}fluoro-2-deoxyglucose positron emission tomography (FDG-PET), which capitalizes on enhanced glucose uptake in tumors (Fletcher et al., 2008).

Metabolic gene expression and metabolomics have been used to identify subclasses among individual human tumors from the same organ (Caro et al., 2012; Terunuma et al., 2014), but it is unknown whether these differences reflect true changes in metabolic activity *in vivo*. Tumor metabolism is regulated by a poorly-defined combination of cell-intrinsic and -extrinsic factors. Oncogene expression is sufficient to reprogram some aspects of nutrient utilization, suggesting that cell-autonomous metabolism is driven in part by the oncogenotype (Gao et al., 2009; Ji et al., 2007; Son et al., 2013). Altered perfusion from abnormal tumor vasculature is believed to be a major extrinsic driver of metabolism through effects on oxygen and substrate delivery (Guillaumond et al., 2013). Other extrinsic effects include metabolic competition or cooperativity among stromal, immune and tumor cells (Pavlides et al., 2009; Sonveaux et al., 2008). A full accounting of tumor metabolism will need to consider extrinsic influences in addition to the complexity imposed by the oncogenotype.

The tumor microenvironment is difficult to model *ex vivo*, and this limits the use of culture-based systems to infer the metabolism of intact tumors. Stable isotopes (e.g. ^{13}C) are widely

used to investigate cellular metabolism because patterns of ^{13}C enrichment downstream of a labeled nutrient encode information about pathway activity (Buescher et al., 2015). The safety of ^{13}C makes this approach feasible in humans. A few studies have provided ^{13}C-labeled nutrients to cancer patients during tumor resection, then analyzed ^{13}C enrichment in metabolites extracted from the tumor. In gliomas and brain metastases, infusions of [U-^{13}C]glucose revealed metabolism of glucose through both glycolysis and the TCA cycle (Maher et al., 2012). In NSCLC, introducing [U-^{13}C]glucose as a bolus revealed that both glycolysis and TCA cycle metabolism were active in the tumor (Fan et al., 2009). Pyruvate carboxylase (PC), the enzyme converting pyruvate to oxaloacetate (OAA), was highly expressed in NSCLC and contributed to labeling differences between tumor and lung (Sellers et al., 2015).

None of these reports assessed heterogeneity within or between tumors, or the influence of cell-extrinsic factors on metabolism. Here we incorporated clinical imaging to provide quantitative information about glucose metabolism and the tumor environment in NSCLC from 9 untreated patients. We demonstrate that these tumors are heterogeneous with respect to glucose utilization, and that areas of metabolic heterogeneity between and within tumors can be predicted by assessing tissue perfusion pre-operatively.

RESULTS

Workflow for pre-operative imaging, intra-operative ^{13}C-glucose infusion and sample selection

Prior to surgery, tumors were assessed by FDG-PET and multiparametric MRI (mpMRI) (Figure 1A). MpMRI consisted of T2-weighted imaging for anatomy; diffusion-weighted imaging (DWI) to determine the apparent diffusion coefficient (ADC), a surrogate for cellularity; and dynamic contrast-enhanced MRI (DCE-MRI), which measures time-dependent entry of a contrast agent and is used to assess perfusion (Koh and Collins, 2007; Yankeelov and Gore, 2009). Multidisciplinary conferences involving the research team, surgeon and radiologist were held to discuss the images and plan tissue sampling. On the day of surgery, the patient had an intravenous catheter placed into each arm. One was used to deliver 8 grams of [U-^{13}C]glucose over 10 minutes, followed by a continuous infusion of 8 grams/hour for an average of 3 hours until the lobectomy was performed. The other was used to withdraw blood samples for analysis of ^{13}C enrichment in plasma glucose. This approach achieves a persistent state of high enrichment of plasma glucose (Maher et al., 2012). After removal of the lobe, the tissue was oriented to identify anatomic landmarks and dissected to procure specific fragments prioritized by pre-surgical imaging. The fragments were rinsed, frozen, and subjected to histological, molecular and metabolic analysis.

Imaging and ^{13}C data from a 59 year-old female smoker with a grade 3 adenocarcinoma (patient 1) are in Figure 1B–E. This tumor exceeded 22 cm^3 and was FDG-PET avid, demonstrating heterogeneous FDG signal and $SUV_{max} > 10$ (Figure 1B, Table 1). Plasma glucose enrichment exceeded 30% for 2h (Figure 1C). Histology revealed the tumor to have abundant staining for Ki67, a marker of cell proliferation, and CD31, a marker of tumor vasculature (Figure 1D). Metabolites were extracted from lung and from an FDG-avid, ADC-low (i.e. highly cellular) tumor fragment. For an intuitive display of how ^{13}C labeling

compared between the tumor and lung, average relative fractional enrichments (i.e. fractional enrichment in tumor/fractional enrichment in lung) are shown for several metabolites. Glucose and the glycolytic intermediate 3-phosphoglycerate (3-PG) had somewhat lower fractional enrichments in the tumor, but all other glucose-derived metabolites, including lactate and TCA cycle-derived intermediates (citrate, glutamate and malate) were more enriched in the tumor (Figure 1E; full ^{13}C distributions in Figure S1). Thus, in this tumor, high FDG uptake correlated with enhanced contribution of glucose to lactate and TCA cycle intermediates.

Comparison of bolus and continuous infusions of [U-^{13}C]glucose administration

Administering ^{13}C glucose as one or more boluses rather than a continuous infusion has been used to assess tumor metabolism in humans and mice (Fan et al., 2009; Sellers et al., 2015; Yuneva et al., 2012). Boluses have the advantage of reduced cost and ease of administration. On the other hand, infusions may lead to improved ^{13}C signal, better evaluation of complex pathways requiring persistent ^{13}C exposure, and the possibility of achieving isotopic steady state to simplify analysis (Marin-Valencia et al., 2012). Analysis of the TCA cycle is complicated by the fact that labeling depends not only on the route of entry but also the number of times the cycle has turned. To compare these methods, we assessed labeling data obtained from brief vs. prolonged periods of ^{13}C exposure. Patient 2 received an 8g bolus of [U-^{13}C]glucose, followed shortly thereafter by resection. This produced a rapid rise in glucose enrichment, but no plateau in the circulation (Figure S2A). Patient 3 received an 8g bolus prior to anesthesia followed by another 8g bolus one hour before surgery (Figure S2B). As in patient 1, enrichments in lactate (M+3) and TCA cycle intermediates (M+2 citrate, glutamate and malate) were higher in the tumor than the lung of patients 2 and 3 (Figure S2C). The relative enrichment of these species was not improved by patient 1's longer infusion, but the absolute enrichments were lower in patients 2 and 3, resulting in poor signal for higher-order labeling (e.g. M+3–4 in citrate and malate, Figure S2D,E). M+1 isotopologues were also better represented after persistent ^{13}C glucose exposure; this form of labeling likely arises after multiple turns of the TCA cycle (Figure S2F,G). Thus, boluses are sufficient to detect abundant isotopologues but compromise assessment of other isotoplogues. For these reasons, we used infusions in patients 4–9.

Enhanced anaerobic and aerobic glucose metabolism in NSCLC

Table 1 and Figure S3 contain clinical and histological information from the 9 patients. The tumors were heterogeneous in their TNM stage, grade and SUV$_{max}$. Molecular analysis of *EGFR* and *KRAS* revealed *EGFR* mutations in four patients and *KRAS* mutations in two; three tumors did not contain mutations in either gene. The tumors also displayed a wide range of stromal content, microvessel density and MIB-1 fraction (Table 1). Plasma glucose enrichments showed the expected rapid rise in ^{13}C fractional enrichment due to the bolus, followed by a plateau during the infusion (Figure S4). Complete ^{13}C isotopologues from all tissue fragments are in Table S1. Relative fractional enrichments are shown for several informative metabolites (averages in Figure 2A and data from individual fragments in Figure 2B). All lung samples demonstrated enrichment of intermediates from glycolysis and the TCA cycle, indicating that benign lung uses both pathways (Table S1). These intermediates were also labeled in all tumors. Importantly, although there was substantial

variability in ^{13}C labeling, the variability among patients far exceeded the variability among independent samples obtained from the same tumor, indicating that this technique detects biological variation in human tumor metabolism (Figure 2C).

Despite the fact that all tumors displayed FDG uptake by PET, glucose fractional enrichment was lower on average in tumor than lung, as previously reported (Fan et al., 2009). Lactate, by contrast, was more enriched in tumor fragments, indicating a greater propensity to convert [U-^{13}C]glucose to [U-^{13}C]lactate than non-cancerous lung. Several metabolites related to the TCA cycle (e.g. M+2 isotopologues of acetyl-CoA, citrate, glutamate and malate) were also more enriched in the tumors (Figure 2A,B).

Although these M+2 enrichments likely reflect entry of label into the TCA cycle via the pyruvate dehydrogenase (PDH) reaction, mass spectrometry does not provide positional ^{13}C information. This potentially confounds the interpretation of qualitative assessment of MS isotopologues, particularly when the overall enrichment is low. M+2 isotopologues in citrate, etc. may therefore reflect PDH-dependent labeling during the first turn of the cycle, multiple turns of the cycle, or the combined effects of PC-dependent entry and multiple turns. To limit the assumptions needed to interpret the data, we analyzed several fragments by ^{13}C NMR spectroscopy, which definitively assigns ^{13}C positions. These spectra revealed prominent 4–5 doublets in carbon 4 of glutamate, a pattern requiring PDH activity. This doublet was much more prominent in tumor than lung (Figure 3A, S5A), and labeling of the 4–5 doublet relative to the C4 singlet was highly correlated with fractional enrichments of M+2 in citrate and glutamate (Figure 3B). These observations indicate that enhanced TCA cycle labeling in tumors reflects entry of uniformly labeled acetyl-CoA into the cycle via PDH. Strong correlations between mass isotopologues lactate M+3 and citrate M+2, and between citrate M+2 and malate M+2 indicate that glycolysis, PDH and TCA cycle activity are linked in the tumors (Figure 3C). To rule out artificial inflation of ^{13}C labeling by metabolite pool depletion (Buescher et al., 2015), we also analyzed metabolite abundance. Glucose was less abundant in the tumors, lactate was more abundant, and TCA cycle intermediates displayed no consistent trend (Figure S5B,C). Thus, human NSCLC tumors display enhanced carbon flow through PDH and the TCA cycle compared to adjacent lung.

Lung tumors contain increased expression of PC and have evidence of enhanced flux through this anaplerotic enzyme as assessed by qualitative assessment of ^{13}C enrichment (Sellers et al., 2015). PC converts [U-^{13}C]pyruvate into OAA M+3, which can condense with unlabeled acetyl-CoA to produce citrate M+3 and equilibrate with malate to produce malate M+3. Fractional enrichments of malate, citrate and glutamate M+3 were higher in tumor than lung (Figure 3D), although the absolute abundance of these species was much lower than PDH-derived isotopologues (Table S1). Citrate M+5, the condensation product of OAA M+3 and acetyl-CoA M+2, was barely detectable, likely because of the low absolute enrichment in OAA and acetyl-CoA. TCA cycle turnover was assessed by analyzing the fractional enrichment of citrate M+1 and malate M+1, both of which were over-represented in the tumors (Figure 3E). Therefore, the prominence of M+2 isotopologues is not an artifact of reduced cycle turnover.

To extend the analysis beyond qualitative assessment, we used tcaSIM, a computational tool that simulates metabolic networks involving glycolysis, the TCA cycle, fatty acid oxidation, anaplerosis and other activities. The utility of this tool is enhanced by the higher and more complex labeling data provided by steady-state rather than bolus infusions. tcaSIM can be used to identify relative fluxes that best account for experimental labeling data derived from multiple metabolites simultaneously. This approach avoids pitfalls associated with simple qualitative analysis, such as the possibility that enhanced ^{13}C labeling in TCA cycle intermediates arises from high enrichment in upstream metabolites rather than *bona fide* flux changes. Modeling indicated that both PC and PDH fluxes, relative to citrate synthase flux used as a reference, were elevated in the tumors. PDH rather than PC dominated pyruvate entry into the TCA cycle in both tumor and normal lung (Figure 3F). The magnitude of PDH flux was positively correlated with the MIB-1 fraction (Figure S5D).

Evidence for lactate utilization by NSCLC tumors in humans and mice

Although acetyl-CoA enrichment was higher in tumors than lung (Figure 2A), the absolute enrichment was low (Figure 4A). This prompted us to examine whether other blood-borne metabolites contribute to tumor metabolism. Lactate circulates at levels of 1–2 mM and is a fuel for cancer cells under some conditions (Guillaumond et al., 2013; Kennedy et al., 2013; Sonveaux et al., 2008). To examine the impact of circulating lactate on tumor metabolism, we first compared fractional enrichments between lactate and the glycolytic intermediates 3-PG and PEP in tumor and lung from all patients. In lung fragments, 3-PG and PEP enrichments were similar to lactate enrichment, and the average ratio of lactate M+3 to 3-PG or PEP M+3 was almost exactly 1.0 (Figure 4B). This is expected if lactate arises from glycolysis in the lung. In contrast, lactate enrichment in many tumor fragments exceeded 3PG or PEP enrichment (Table S1), and the average lactate M+3 exceeded 3-PG or PEP M +3 by ~40% (Figure 4B). Excess labeling was also propagated into the TCA cycle, as the ratio of enrichment of citrate M+2 to 3-PG or PEP M+3 was higher in tumors (Figure 4B). These findings implied that additional labeled substrates contributed to tumor lactate. The most obvious candidate was lactate itself, because lactate imported from the plasma would feed the tumor lactate pool and could provide carbon to the TCA cycle (Figure 4C). Indeed, [U-^{13}C]glucose infusion led to measurable amounts of circulating [U-^{13}C]lactate (Figure 4D, Table S1). Because plasma lactate enrichments were lower than glucose enrichments in both the plasma and tumor, metabolism of ^{13}C-lactate in the tumor would dilute enrichment in acetyl-CoA and other metabolites relative to tumor glucose enrichment. Given our confirmation by NMR that M+2 isotopologues primarily reflect entry and passage of [U-^{13}C]acetyl-CoA through the TCA cycle, if the fractional M+2 enrichment of TCA cycle intermediates exceeded M+3 in 3-PG and PEP, this would be consistent with contribution of lactate to TCA cycle metabolism. This relationship was observed in several patients, including patient 1 (Figure 4E, Table S1). Others like patient 5 demonstrated a pattern of progressive decline in labeling from glucose to all downstream intermediates, similar to the lung (Figure 4E). These data suggest that some human lung tumors may use lactate as a carbon source.

To examine lactate metabolism directly, mice bearing subcutaneous xenografts derived from cell lines bearing mutations in *KRAS* (A549 cells, G12S mutation) or *EGFR* (HCC827 cells,

E746-A750 deletion) were infused with [2-^{13}C]lactate. This led to rapid and persistent enrichment of the circulating lactate pool (Figure 4G), and some enrichment in glucose as lactate was used as a gluconeogenic precursor (Figure 4F). Lactate within these tumors was significantly labeled (Figure 4G). Enrichment in citrate, malate and glutamate exceeded enrichment of 3-PG, indicating that these metabolites contained ^{13}C from imported lactate rather than from labeled glucose.

Individual NSCLC tumors display heterogeneous degrees of glucose metabolism predicted by an MRI marker of perfusion

The extensive metabolic heterogeneity among tumors prompted an examination of factors regulating glucose metabolism. The availability of DCE MRI data in all patients provided an opportunity to examine the influence of perfusion on tumor metabolism. We first assessed mean signal intensity of DCE images by manually drawing a region of interest (ROI) of a slice chosen for maximal tumor diameter. Tumors were easily dichotomized by qualitative DCE assessment, with several displaying higher time-dependent contrast enhancement and the rest displaying lower enhancement (Figure 5A). DCE data were also analyzed as the initial area under the curve 60 seconds after contrast administration (iAUC60, Figure 5B). This parameter was previously demonstrated to be stable in human NSCLC over at least one week (Ng et al., 2010), similar to the period of time between imaging and resection in our patients (1–8 days). Analysis of fractional enrichment revealed that metabolites from well-perfused tumors were nearly indistinguishable from adjacent lung, whereas tumors with low iAUC60 values had, on average, higher enrichments compared to either benign lung or tumors with high iAUC60 values (Figure 5C). Modeling ^{13}C enrichment data showed that PDH flux was approximately three times higher in tumors with low contrast enhancement, whereas PC flux was no different between the groups (Figure 5D).

To test whether regions of metabolic heterogeneity existed within individual tumors, we used DCE MRI to identify anatomic regions of differential contrast enhancement, then selected regions of high and low contrast uptake from the same tumor for metabolite extraction and ^{13}C enrichment analysis. Patient 8 was a non-smoker with an *EGFR*-mutated adenocarcinoma measuring 16.1 cm^3 and a high SUV$_{max}$ (Figure 5E, Table 1). Although analysis of DCE MRI of the tumor as a whole identified this as a well-perfused mass (Figure 5A), DCE characteristics were dramatically different between the superior and inferior regions (Figure 5E). Fragments obtained from the superior and inferior aspects were sectioned into three smaller fragments, extracted, and analyzed for ^{13}C enrichment. Enrichments in the less well-perfused inferior aspect of the tumor were significantly higher than those in the superior aspect (Figure 5F). Both NMR spectroscopy and modeling of mass spectrometry data confirmed differential metabolism in these two areas of the tumor (Figure S6). Patient 9 had a 3.8 cm^3 adenocarcinoma with a low SUV$_{max}$ (Table 1) and relatively poor DCE signal throughout (Figure 5A). However, subtle differences were detected, indicating modestly enhanced signal in the posterior compared to the medial region (Figure S7A,B). As in patient 8's larger and more FDG-avid tumor, fragments isolated from these two regions displayed differences in ^{13}C enrichment, with the region of higher DCE signal demonstrating small reductions in ^{13}C enrichment of lactate, citrate and other metabolites (Figure S7C). Thus, DCE-based assessment of perfusion predicts the extent of glucose's

contribution to central metabolism across a clinically-relevant range of perfusion and SUV_{max}.

To generate more insight into the relationship between DCE phenotypes and metabolism, RNA sequencing was performed on fragments from several tumors. The fragments were then clustered according to their gene expression signatures, using all detected transcripts or a subset of 2,756 genes related to metabolism (Figure 6A)(Possemato et al., 2011). In neither of these unsupervised analyses did the fragments segregate according to the perfusion phenotype. However, gene set enrichment analysis (GSEA) revealed enhanced expression of genes related to glycolysis, oxidative phosphorylation and the TCA cycle in fragments with low DCE signal, whereas fragments with high DCE signal were enriched for genes related to other nutrients, with many of the 20 most-enriched gene sets related to the lysosome and amino acid metabolism (Figure 6B,C). Thus, areas of differential DCE signal display altered patterns of gene expression and altered utilization of glucose-derived carbon to supply central metabolism.

DISCUSSION

Here we coupled [U-^{13}C]glucose infusions with FDG-PET and mpMRI to assess glucose fates in NSCLC, compare metabolism to adjacent lung, and identify aspects of tumor biology that predict metabolism *in vivo*. Our work extends other recent efforts to analyze human tumor metabolism with isotope tracers. In particular, two previous studies used a bolus of ^{13}C-glucose prior to resection to assess NSCLC metabolism (Fan et al., 2009; Sellers et al., 2015). Like them, we observed evidence of enhanced glycolysis and TCA cycle activity in the tumors, and concluded that enhanced pyruvate carboxylation differentiates NSCLC from lung. Our work adds to these studies in several ways. First, we report the molecular and histological characteristics of tumors in the study. This allowed us to demonstrate that enhanced glucose oxidation is observed across diverse histological subtypes and oncogenotypes. Second, we applied a computational assessment of glucose metabolism after persistent exposure to a continuous source of isotope in the circulation. Ultimately, this provided information about both carbon entry into and processing by the TCA cycle, as well as an assessment of the extent to which glucose and other fuels supply oxidative metabolism. Third, integrating multimodality imaging with ^{13}C-derived data allowed us to compare metabolic markers with other biological features, particularly tissue perfusion. Because these features are suspected to influence metabolism, our approach provides information about the drivers of metabolic complexity in human NSCLC.

Several practicalities of these human studies bear mention. The surgical procedure requires ligation of the pulmonary artery for 15–30 minutes prior to resection of the diseased lobe. During this time, the lobe and tumor depend on bronchial and collateral circulation for nutrient delivery. Evidence indicates that this did not significantly alter oxygenation of the tumor. The bronchial circulation carries highly oxygenated blood and accounts for a greater contribution to total NSCLC blood flow than the pulmonary circulation (Nguyen-Kim et al., 2015). Inspection of ^{13}C labeling indicated hallmarks of enhanced rather than suppressed TCA cycle metabolism, arguing against severe oxygen limitation. These markers persisted even in the occasional patient (not shown) in which the ligation lasted for several hours.

Thus, although total blood flow was likely reduced by pulmonary artery ligation, this did not prevent the tissue from engaging in oxidative metabolism.

A technical limitation is that the method requires fragments large enough for ^{13}C studies (~50 mg), inevitably leading to a mixture of malignant and stromal cells. We used pre-surgical imaging and gross inspection of the tumor to choose fragments composed primarily of viable, malignant cells, and histology to confirm this. Although individual tumors contained variable contributions of non-malignant cells, the consistency of key features across the cohort (e.g. enhanced labeling of TCA cycle intermediates) strongly implies that these features are consequences of the malignant cells. Also, some aspects of the modeling assume homogeneity within each fragment with respect to glucose metabolism. Although it is unknown to what extent stromal cells impact metabolic homogeneity within the fragment, we note that the qualitative assessment of labeling and the modeled acetyl-CoA enrichment agreed very well with each other.

Despite these complexities, it was possible to draw several conclusions. First, the data strongly suggest that glycolysis and glucose oxidation via PDH and the TCA cycle are enhanced in NSCLC relative to adjacent benign lung. We observed this phenotype in tumors with mutations in either *EGFR* or *KRAS*, and presumably in other oncogenic drivers not detected by our molecular analysis. The effect of specific oncogenic mutations is unclear from the current cohort. Although the two *KRAS*-mutant tumors had high levels of ^{13}C labeling, both also had low-DCE signal, which independently predicted high ^{13}C labeling across the entire group. The overall impression is that multiple oncogenic drivers can specify a phenotype of robust glucose oxidation *in vivo*. This is consistent with the observation that enhanced glucose metabolism is a shared consequence of many tumorigenic mutations in cultured cancer cells. However, the relationship between glycolysis and glucose oxidation in live tumors has been difficult to ascertain. A common perception is that avid ^{18}FDG uptake implies enhanced glycolysis and suppressed glucose oxidation, analogous to the conventional understanding of the Warburg effect (Warburg, 1956). Our data provide strong evidence against the concept of a "switch" from oxidative to glycolytic metabolism in NSCLC. Several tumors in the study had SUV_{max} values exceeding 10, yet there was no evidence of suppressed glucose oxidation. We conclude that enhanced glucose uptake in ^{18}FDG-PET-positive lung tumors supplies enhanced glucose oxidation. Increasing the cohort size will make it possible to test whether particular mutations elicit specific effects on glucose metabolism.

Second, entry of ^{13}C into the TCA cycle was dominated by PDH. PDH-dependent labeling of TCA cycle metabolites was observed in all tumors and was enhanced on average relative to benign lung. Most cancer cell lines also use PDH to supply carbon from glucose to the TCA cycle, although this enzyme is dispensable for survival and proliferation when other nutrients are available in culture (Rajagopalan et al., 2015). In our cohort, PDH activity correlated with Ki67 staining, suggesting that PDH functions in proliferating malignant cells.

Third, the tumors displayed low enrichment in acetyl-CoA relative to glucose. This likely indicates that additional substrates enter the metabolic network between glucose and the

TCA cycle. Although glucose is a prominent energy source, emerging evidence indicates that tumor cells oxidize other nutrients as well, and in some circumstances may prefer alternative fuels to glucose (Boroughs and DeBerardinis, 2015; Mashimo et al., 2014). Other potential carbon sources include fatty acids, amino acids, ketones and macromolecules scavenged from the extracellular space. Our data suggest that lactate, typically viewed as a waste product of cancer cells, can be used as a respiratory substrate by NSCLC tissue. Lactate is abundant and is taken up by monocarboxylate transporters (MCTs), several of which are expressed in NSCLC (Eilertsen et al., 2014). Lactate dehydrogenases (LDH) catalyze NAD^+/NADH-dependent exchanges between lactate and pyruvate. Although all LDH isoforms catalyze this reaction in both directions, isoforms containing B subunits encoded by *LDHB* may favor conversion of lactate to pyruvate and are highly expressed in tissues that use lactate as a fuel. *LDHB* is highly expressed in a subset of NSCLC tumors and cell lines and correlates with poor survival in adenocarcinoma (McCleland et al., 2013). It has been proposed that lactate is used as a respiratory substrate in well perfused areas of solid tumors, with less perfused areas of the same tumors converting glucose to lactate and secreting it (Sonveaux et al., 2008). Our data do not document net lactate consumption and do not discriminate regional localization of lactate oxidation. However, we do observe that, on average, the contribution of substrates other than [U-^{13}C]glucose to the TCA cycle was accentuated in regions of high DCE signal. The data suggest a role for PET probes based on lactate and other fuels to help define nutrient preferences in human NSCLC and determine their regulation by the oncogenotype, the microenvironment, and other factors.

Fourth, a key finding was that the metabolic variability among tumors could be predicted by DCE. Tumors with high DCE signal were similar to normal lung in terms of ^{13}C enrichment, while tumors with lower signal had enhancements of essentially all isotopologues related to the TCA cycle via either PDH or PC. This implies that the predominant metabolic phenotype observed in human NSCLC (enhanced ^{13}C labeling of TCA cycle intermediates) is related to perfusion. It is unclear whether altered perfusion dictates metabolic activity or whether reduced perfusion and altered metabolism occur in parallel downstream of other factors. In support of the former hypothesis, when considered in light of the low tumor acetyl-CoA enrichment and RNA-Seq data, the relationship between ^{13}C enrichment and DCE suggests that perfusion alters the contributions of various fuels to the TCA cycle (Figure 6D). Specifically, high-DCE tumors may oxidize multiple substrates simultaneously, but if perfusion becomes compromised in low-DCE tumors, the contribution of glucose to the TCA cycle rises relative to competing substrates. This may simply reflect the fact that glucose exceeds fat and protein in terms of energy produced per unit of oxygen consumed, and may be preferable in states of modestly reduced perfusion. An alternative but not mutually exclusive possibility is that less-abundant nutrients become depleted in areas of reduced perfusion, whereas glucose remains available by virtue of its high concentration and diffusivity. A similar hypothesis was proposed to explain how interactions between tumor cells and the microenvironment favor a glucose-avid phenotype (Gatenby and Gillies, 2004). In this setting, enhanced glucose metabolism may be required to provide energy and synthetic precursors to offset reduced availability of other fuels and macromolecules from the circulation.

We capitalized on the excellent spatial resolution of DCE MRI to perform regional analysis within individual tumors. This produced evidence of regional heterogeneity of metabolic flux in solid tumors. Notably, the data suggest that the influence of perfusion may override the intrinsic metabolic preferences set by the genetics of the tumor. For example, patient 8's tumor contained an L858R mutation in *EGFR*, yet metabolic activity varied considerably across the tumor in correlation with the DCE phenotype. A key emerging question is whether metabolic vulnerabilities also display such striking regional heterogeneity within individual tumors. This would have major implications for the prospects of metabolic therapy in cancer.

In summary, we report the power and practicality of combining clinical imaging and ^{13}C enrichment in human cancer. Our data suggest that tumor metabolism is significantly and predictably regulated by the microenvironment, and that local alterations of metabolism can be identified prior to surgery. This technique enables a rational approach to sample procurement. Given the ever-expanding repertoire of context-specific metabolic pathways in cancer cells (Boroughs and DeBerardinis, 2015), this method should greatly increase the information yield of experiments involving isotope tracers. It should now be possible to identify and pre-select regions using alternative substrates to supply the TCA cycle, and to test specific hypotheses related to interactions between the microenvironment and metabolic preferences. Because DCE and other acquisition methods of mpMRI are suitable for mouse models of cancer, it will also be possible to use this approach in experimental systems where the cost of infusions is low and control of experimental parameters is high.

EXPERIMENTAL PROCEDURES

Additional detail is in Extended Experimental Procedures

Clinical Protocol—Nine patients with untreated NSCLC were enrolled in an IRB protocol after obtaining informed consent. On the day of surgery, [U-^{13}C]glucose was introduced as described (Maher et al., 2012). Standard surgical procedures were followed with the majority of cases being robotic lobectomies. Tissue fragments were immediately frozen in liquid nitrogen. Histological analyses were conducted by pathologists blinded to the metabolic results. Exons 18–21 of *EGFR* were bi-directionally Sanger sequenced using lab-developed primers. Mutation analysis for *KRAS* codons 12, 13, 61 and 146 was performed on a Sequenom Mass ARRAY system (MALDI-TOF) with manual calling.

Multi-parametric Magnetic Resonance Imaging (mpMRI)—MRIs occurred 8 or fewer days before surgery. Coronal and axial T2-weighted images were used to localize the lesion and acquire measurements. DCE and DWI were performed within the same examination.

Mass Spectrometry and NMR Spectroscopy—Blood obtained during infusions was used to measure plasma glucose enrichment as described (Maher et al., 2012). Tissue samples (50–100mg) were added to 50:50 methanol:water for extraction. GC/MS and NMR were performed as described (Cheng et al., 2011; Maher et al., 2012).

Mouse studies—All procedures were approved by UT Southwestern's Animal Care and Use Committee in accordance with the *Guide for the Care and Use of Laboratory Animals*. One million A549 or HCC827 cells were injected into the flanks of *Ncr* nude mice. Before infusions, mice were fasted for 16 hours, then 27 gauge catheters were placed in the lateral tail vein under anesthesia. A 10% weight:weight aqueous solution of [2-^{13}C]lactate (Cambridge Isotope Laboratories) was infused via syringe pump for 120 minutes, at a rate of 150μl over 10 minutes and 2μl/min until the end of the infusion. Blood samples of ~50μl were obtained periodically. Animals were euthanized at the end of the infusion, then tumors were harvested, rinsed briefly in cold saline and frozen in liquid nitrogen.

RNA-sequencing—Tumor samples were homogenized and RNA was extracted. Three μg of RNA was processed for library preparation and sequencing. Raw reads were aligned to human genome assembly hg19. A set of 2,756 human metabolic genes (Possemato et al., 2011) was used for GSEA to define differentially expressed pathways between samples with high or low DCE signal. RNA-seq data was deposited in the Gene Expression Omnibus database under GSE74484.

Statistics—Patient-matched samples were analyzed by paired Student's t-test. Inter-tumor analysis of contrast enhancement and relative fractional enrichments was analyzed by unpaired Student's t-tests. Correlation plots were analyzed with Pearson's product-moment correlation coefficients of the trendlines. All data were considered significant if $p < 0.05$.

Supplementary Material

Refer to Web version on PubMed Central for supplementary material.

Acknowledgments

References

Boroughs LK, DeBerardinis RJ. Metabolic pathways promoting cancer cell survival and growth. Nature cell biology. 2015; 17:351–359. [PubMed: 25774832]

Buescher JM, Antoniewicz MR, Boros LG, Burgess SC, Brunengraber H, Clish CB, DeBerardinis RJ, Feron O, Frezza C, Ghesquiere B, et al. A roadmap for interpreting C metabolite labeling patterns from cells. Current opinion in biotechnology. 2015; 34:189–201. [PubMed: 25731751]

Caro P, Kishan AU, Norberg E, Stanley IA, Chapuy B, Ficarro SB, Polak K, Tondera D, Gounarides J, Yin H, et al. Metabolic signatures uncover distinct targets in molecular subsets of diffuse large B cell lymphoma. Cancer cell. 2012; 22:547–560. [PubMed: 23079663]

Cheng T, Sudderth J, Yang C, Mullen AR, Jin ES, Matés JM, DeBerardinis RJ. Pyruvate carboxylase is required for glutamine-independent growth of tumor cells. Proceedings of the National Academy of Sciences. 2011; 108:8674–8679.

DeBerardinis RJ, Lum JJ, Hatzivassiliou G, Thompson CB. The Biology of Cancer: Metabolic Reprogramming Fuels Cell Growth and Proliferation. Cell Metabolism. 2008; 7:11–20. [PubMed: 18177721]

Eilertsen M, Andersen S, Al-Saad S, Kiselev Y, Donnem T, Stenvold H, Pettersen I, Al-Shibli K, Richardsen E, Busund LT, et al. Monocarboxylate transporters 1–4 in NSCLC: MCT1 is an independent prognostic marker for survival. PloS one. 2014; 9:e105038. [PubMed: 25225794]

Fan TW, Lane AN, Higashi RM, Farag MA, Gao H, Bousamra M, Miller DM. Altered regulation of metabolic pathways in human lung cancer discerned by (13)C stable isotope-resolved metabolomics (SIRM). Molecular cancer. 2009; 8:41. [PubMed: 19558692]

Fletcher JW, Djulbegovic B, Soares HP, Siegel BA, Lowe VJ, Lyman GH, Coleman RE, Wahl R, Paschold JC, Avril N, et al. Recommendations on the Use of 18F-FDG PET in Oncology. Journal of Nuclear Medicine. 2008; 49:480–508. [PubMed: 18287273]

Gao P, Tchernyshyov I, Chang TC, Lee YS, Kita K, Ochi T, Zeller KI, De Marzo AM, Van Eyk JE, Mendell JT, et al. c-Myc suppression of miR-23a/b enhances mitochondrial glutaminase expression and glutamine metabolism. Nature. 2009; 458:762–765. [PubMed: 19219026]

Gatenby RA, Gillies RJ. Why do cancers have high aerobic glycolysis? Nat Rev Cancer. 2004; 4:891–899. [PubMed: 15516961]

Guillaumond F, Leca J, Olivares O, Lavaut MN, Vidal N, Berthezène P, Dusetti NJ, Loncle C, Calvo E, Turrini O, et al. Strengthened glycolysis under hypoxia supports tumor symbiosis and hexosamine biosynthesis in pancreatic adenocarcinoma. Proceedings of the National Academy of Sciences. 2013; 110:3919–3924.

Hanahan D, Weinberg Robert A. Hallmarks of Cancer: The Next Generation. Cell. 2011; 144:646–674. [PubMed: 21376230]

Ji H, Ramsey MR, Hayes DN, Fan C, McNamara K, Kozlowski P, Torrice C, Wu MC, Shimamura T, Perera SA, et al. LKB1 modulates lung cancer differentiation and metastasis. Nature. 2007; 448:807–810. [PubMed: 17676035]

Kennedy KM, Scarbrough PM, Ribeiro A, Richardson R, Yuan H, Sonveaux P, Landon CD, Chi JT, Pizzo S, Schroeder T, et al. Catabolism of exogenous lactate reveals it as a legitimate metabolic substrate in breast cancer. PloS one. 2013; 8:e75154. [PubMed: 24069390]

Koh DM, Collins DJ. Diffusion-weighted MRI in the body: applications and challenges in oncology. AJR American journal of roentgenology. 2007; 188:1622–1635. [PubMed: 17515386]

Maher EA, Marin-Valencia I, Bachoo RM, Mashimo T, Raisanen J, Hatanpaa KJ, Jindal A, Jeffrey FM, Choi C, Madden C, et al. Metabolism of [U-13C]glucose in human brain tumors in vivo. NMR in Biomedicine. 2012; 25:1234–1244. [PubMed: 22419606]

Marin-Valencia I, Yang C, Mashimo T, Cho S, Baek H, Yang XL, Rajagopalan Kartik N, Maddie M, Vemireddy V, Zhao Z, et al. Analysis of Tumor Metabolism Reveals Mitochondrial Glucose Oxidation in Genetically Diverse Human Glioblastomas in the Mouse Brain In Vivo. Cell Metabolism. 2012; 15:827–837. [PubMed: 22682223]

Mashimo T, Pichumani K, Vemireddy V, Hatanpaa KJ, Singh DK, Sirasanagandla S, Nannepaga S, Piccirillo SG, Kovacs Z, Foong C, et al. Acetate is a bioenergetic substrate for human glioblastoma and brain metastases. Cell. 2014; 159:1603–1614. [PubMed: 25525878]

McCleland ML, Adler AS, Deming L, Cosino E, Lee L, Blackwood EM, Solon M, Tao J, Li L, Shames D, et al. Lactate dehydrogenase B is required for the growth of KRAS-dependent lung adenocarcinomas. Clinical cancer research : an official journal of the American Association for Cancer Research. 2013; 19:773–784. [PubMed: 23224736]

Ng CS, Raunig DL, Jackson EF, Ashton EA, Kelcz F, Kim KB, Kurzrock R, McShane TM. Reproducibility of perfusion parameters in dynamic contrast-enhanced MRI of lung and liver tumors: effect on estimates of patient sample size in clinical trials and on individual patient responses. AJR American journal of roentgenology. 2010; 194:W134–140. [PubMed: 20093564]

Nguyen-Kim TD, Frauenfelder T, Strobel K, Veit-Haibach P, Huellner MW. Assessment of bronchial and pulmonary blood supply in non-small cell lung cancer subtypes using computed tomography perfusion. Investigative radiology. 2015; 50:179–186. [PubMed: 25500892]

Pavlides S, Whitaker-Menezes D, Castello-Cros R, Flomenberg N, Witkiewicz AK, Frank PG, Casimiro MC, Wang C, Fortina P, Addya S, et al. The reverse Warburg effect: aerobic glycolysis in cancer associated fibroblasts and the tumor stroma. Cell cycle. 2009; 8:3984–4001. [PubMed: 19923890]

Possemato R, Marks KM, Shaul YD, Pacold ME, Kim D, Birsoy K, Sethumadhavan S, Woo HK, Jang HG, Jha AK, et al. Functional genomics reveal that the serine synthesis pathway is essential in breast cancer. Nature. 2011; 476:346–350. [PubMed: 21760589]

Rajagopalan KN, Egnatchik RA, Calvaruso MA, Wasti AT, Padanad MS, Boroughs LK, Ko B, Hensley CT, Acar M, Hu Z, et al. Metabolic plasticity maintains proliferation in pyruvate dehydrogenase deficient cells. Cancer Metab. 2015; 3:7. [PubMed: 26137220]

Sellers K, Fox MP, Bousamra M 2nd, Slone SP, Higashi RM, Miller DM, Wang Y, Yan J, Yuneva MO, Deshpande R, et al. Pyruvate carboxylase is critical for non-small-cell lung cancer proliferation. The Journal of clinical investigation. 2015; 125:687–698. [PubMed: 25607840]

Son J, Lyssiotis CA, Ying H, Wang X, Hua S, Ligorio M, Perera RM, Ferrone CR, Mullarky E, Shyh-Chang N, et al. Glutamine supports pancreatic cancer growth through a KRAS-regulated metabolic pathway. Nature. 2013; 496:101–105. [PubMed: 23535601]

Sonveaux P, Vegran F, Schroeder T, Wergin MC, Verrax J, Rabbani ZN, De Saedeleer CJ, Kennedy KM, Diepart C, Jordan BF, et al. Targeting lactate-fueled respiration selectively kills hypoxic tumor cells in mice. The Journal of clinical investigation. 2008; 118:3930–3942. [PubMed: 19033663]

Terunuma A, Putluri N, Mishra P, Mathe EA, Dorsey TH, Yi M, Wallace TA, Issaq HJ, Zhou M, Killian JK, et al. MYC-driven accumulation of 2-hydroxyglutarate is associated with breast cancer prognosis. The Journal of clinical investigation. 2014; 124:398–412. [PubMed: 24316975]

Vander Heiden MG. Targeting cancer metabolism: a therapeutic window opens. Nature reviews Drug discovery. 2011; 10:671–684. [PubMed: 21878982]

Warburg O. On respiratory impairment in cancer cells. Science. 1956; 124:269–270. [PubMed: 13351639]

Yankeelov TE, Gore JC. Dynamic Contrast Enhanced Magnetic Resonance Imaging in Oncology: Theory, Data Acquisition, Analysis, and Examples. Current medical imaging reviews. 2009; 3:91–107. [PubMed: 19829742]

Yuneva MO, Fan TW, Allen TD, Higashi RM, Ferraris DV, Tsukamoto T, Mates JM, Alonso FJ, Wang C, Seo Y, et al. The metabolic profile of tumors depends on both the responsible genetic lesion and tissue type. Cell Metab. 2012; 15:157–170. [PubMed: 22326218]
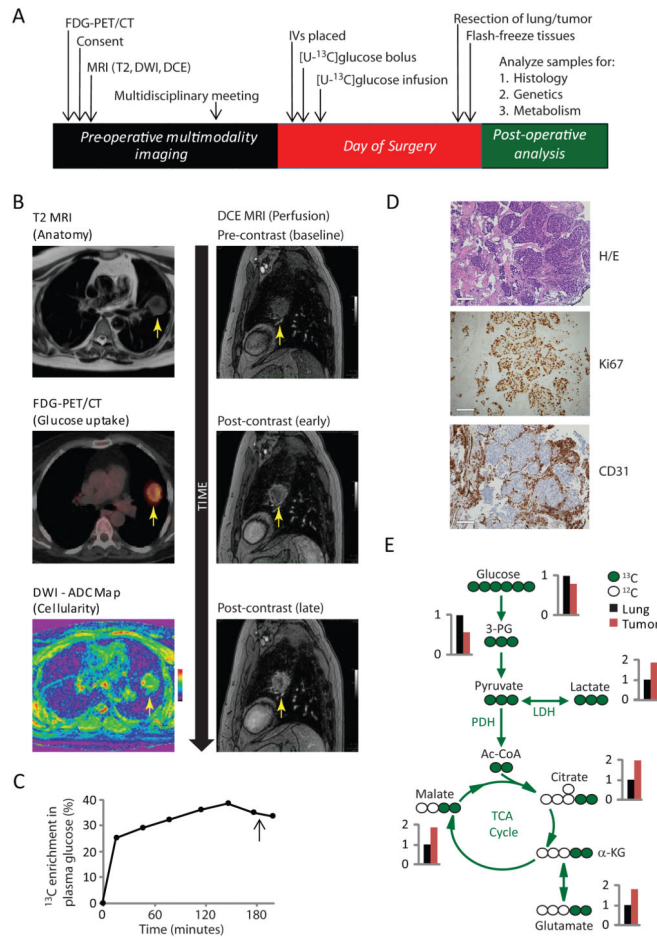
Figure 1. Image-guided assessment of glucose metabolism in human NSCLC

(A) Workflow for clinical study.

(B) Pre-operative imaging of patient 1. FDG-PET/CT was obtained prior to enrollment, and all MRI was performed within a single session. Arrows indicate the grade 3 adenocarcinoma.

(C) Plasma glucose enrichment during [U-^{13}C]glucose infusion. The arrow indicates time of resection.

(D) Histological features. Scale bar, 200μm.

(E) Relative fractional enrichment of glycolytic and TCA cycle metabolites. Tumor values were normalized to values from adjacent lung, which were assigned a value of 1.0.

Abbreviations: FDG-PET/CT, Fluorodeoxyglucose-Positron Emission Tomography/ Computed Tomography; DWI, diffusion weighted imaging; DCE, dynamic contrast-enhanced; ADC, Apparent Diffusion Coefficient; H/E, hematoxylin/eosin; Ac-CoA, acetyl-CoA; LDH, lactate dehydrogenase; PDH, pyruvate dehydrogenase.
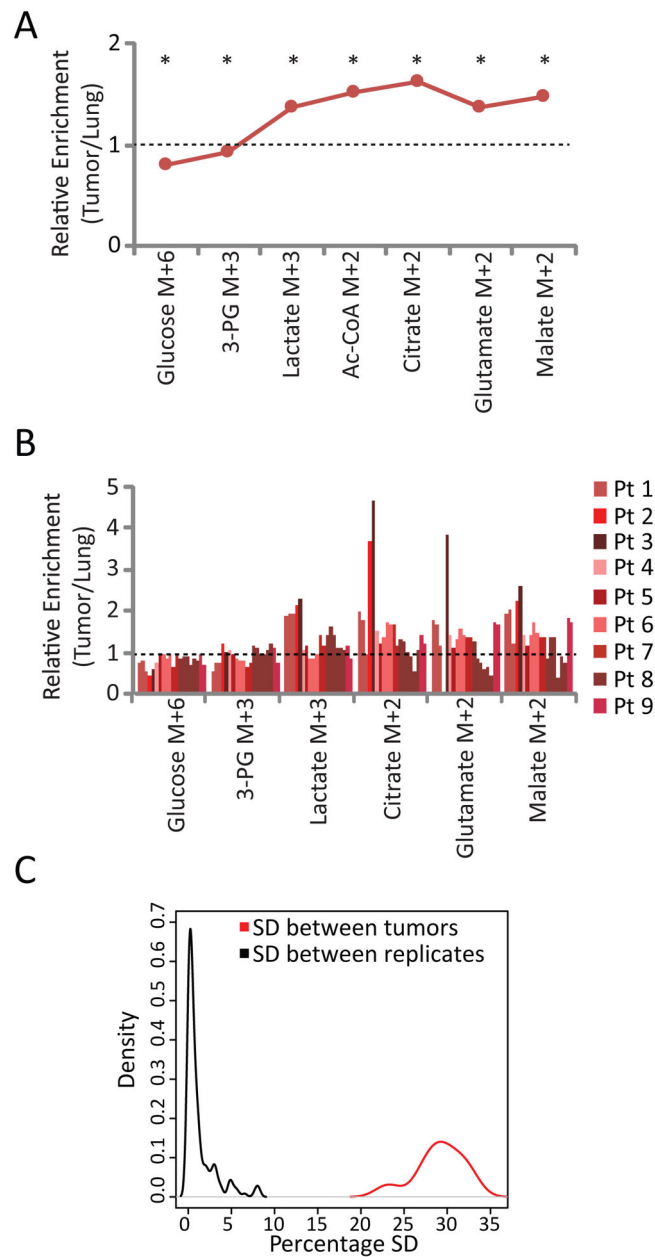
Figure 2. Human NSCLC tumors have enhanced anaerobic and aerobic metabolism compared to adjacent lung

(A) Average relative enrichments (tumor/lung) from 9 patients. Average values were determined using one fragment from each tumor. Acetyl-CoA was not directly measured but estimated from other ^{13}C enrichment data using tcaSIM. *, $p < 0.05$ by Student's paired t-test

(B) Relative enrichments (tumor/lung) of individual fragments from all 9 patients. Note that for most tumors, several fragments were analyzed. No glutamate was detected in patient 2.

(C) Density plots of standard deviations (SD) derived from all ^{13}C enrichments derived from the same localized region of a tumor (SD between replicates) or all ^{13}C enrichments derived from different tumors (SD between tumors). All fractional enrichments were first normalized against the tissue glucose enrichment.
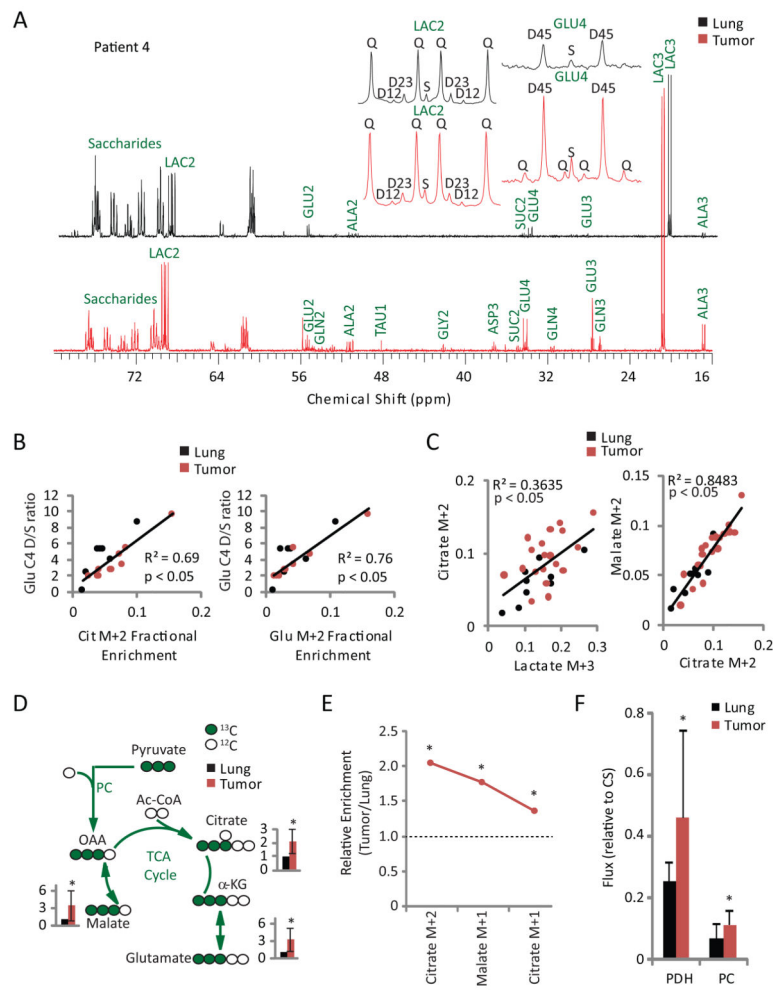
Figure 3. Human NSCLC tumors have enhanced PDH-dependent TCA cycle flux relative to adjacent lung

(A) NMR spectra from the lung and tumor of patient 4. Insets show expansions of multiplets from lactate C2 (LAC2) and glutamate C4 (GLU4). GLN, glutamine; ALA, alanine; TAU, taurine; GLY, glycine; ASP, aspartate; SUC, succinate; S, singlet; D, doublet; Q, quartet (doublet of doublets).

(B) Correlations between NMR-derived and GC/MS-derived labeling features in all fragments for which data were available using both techniques. Data are from 10 tumor fragments and 7 lung fragments from 5 patients. Cit, citrate; Glu, glutamate.

(C) Correlation plots between selected mass isotopologues from 34 tumor and 9 lung fragments.

(D) Tracer scheme illustrating the origin of M+3 species during [U-^{13}C]glucose infusion, with average and SD of measurements from all tumor fragments relative to adjacent lung.

(E) Average relative fractional enrichments (tumor/lung) of isotopologues related to the TCA cycle turnover labeling scheme in Figure S2F.

(F) Fluxes for PDH and PC estimated using tcaSIM. CS, Citrate Synthase.

*, $p < 0.05$ by Student's paired t-test (D, E, F).
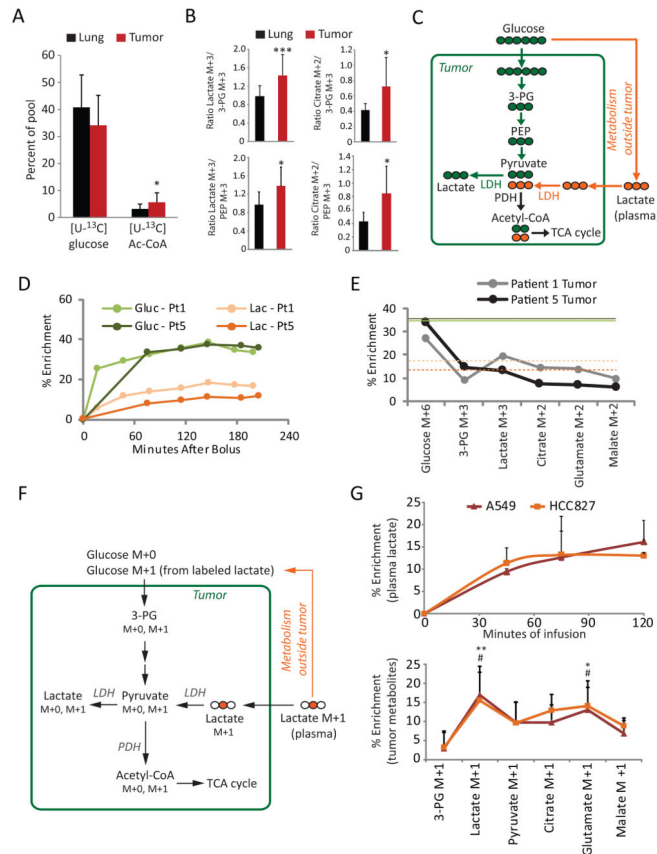
Figure 4. Lactate metabolism in NSCLC in humans and mice

(A) Comparison of major labeled forms of glucose (M+6) and acetyl-CoA (M+2) in tumor and lung. Data are the average and S.D. of all fragments, excluding necrotic tumor fragments. * = p < 0.05 between tumor and lung acetyl-CoA enrichments (paired Student's t-test).

(B) Ratios of labeling in lactate and citrate to the glycolytic intermediates 3-PG and PEP, in lung and tumor. Data are the average and S.D. of all fragments, excluding necrotic tumor fragments. *, p < 0.05; ***, p<0.005 (paired Student's t-test).

(C) Tracer scheme illustrating a tumor lactate pool arising from both glycolysis and lactate import.

(D) Plasma enrichment of glucose M+6 and lactate M+3 in patients 1 and 5.

(E) Percent enrichments of informative mass isotopologues in tumor fragments from patients 1 and 5 (one fragment per patient). Solid green lines indicate glucose M+6 enrichment in the plasma and dashed orange lines indicate lactate M+3 enrichment in the plasma from each patient, as in panel D.

(F) Tracer scheme illustrating [2-^{13}C]lactate infusion in tumor-bearing mice.

(G) *Top*, Plasma enrichment of lactate M+1 during [2-^{13}C]lactate infusions in four mice each with A549 or HCC827 xenografts. *Bottom*, Fractional enrichments of tumor metabolites after infusion with [2-^{13}C]lactate. Data are the average and S.D. of four tumors per cell line. *, p < 0.05 (A549); **, p<0.01 (A549); #, p < 0.05 (HCC827) (One-way ANOVA comparisons to 3-PG).
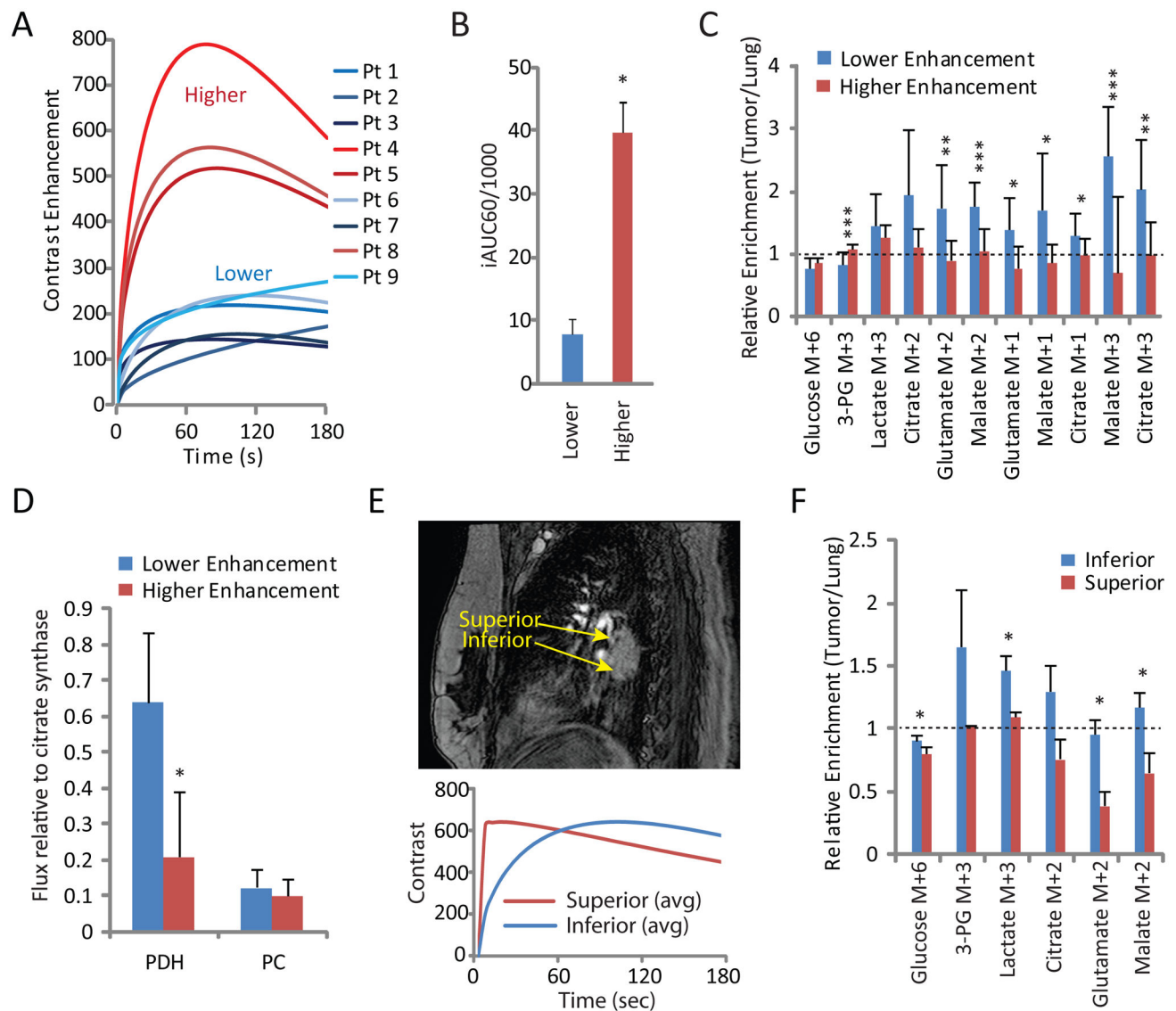
Figure 5. DCE MRI identifies areas of heterogeneous glucose metabolism in NSCLC

(A) DCE data acquired from the region of maximum diameter of each tumor. Tumors could easily be divided into groups with higher and lower DCE signal.

(B) Initial area under the curve for the first 60 seconds (iAUC60) of the time courses in Figure 5A. This semi-quantitative marker of DCE also generates two distinct groups of tumors. Data are average and S.D. of all tumors in the study.

(C) Relative fractional enrichments (tumor/lung) for isotopologues related to glycolysis (3-PG and lactate M+3), PDH and the first TCA cycle turn (Citrate, Glutamate and Malate M +2), subsequent turns of the TCA cycle (Malate and Citrate M+1) and PC activity (Malate and Citrate M+3). Data are average and S.D. of all tumor fragments.

(D) Fluxes for PDH and PC modeled using tcaSIM. Data are average and S.D. of all tumor fragments.

(E) *Top*, Sagittal pre-contrast image of an adenocarcinoma (patient 8). Areas assessed by DCE MRI and sampled for metabolic analysis are indicated. *Bottom*, DCE curves for

superior and inferior aspects of the tumor. The curves plot the average of gamma variate functions fit to three distinct slices from each region of interest.

(F) Relative fractional enrichments (tumor/lung) for isotopologues related to glycolysis (3-PG and lactate M+3), PDH and the first TCA cycle turn (Citrate, Glutamate and Malate M+2). Data are average and S.D. of three fragments each from the superior and inferior aspects of the tumor.

*, $p<0.05$; **, $p<0.01$; ***,$p<0.005$, Student's unpaired t test.
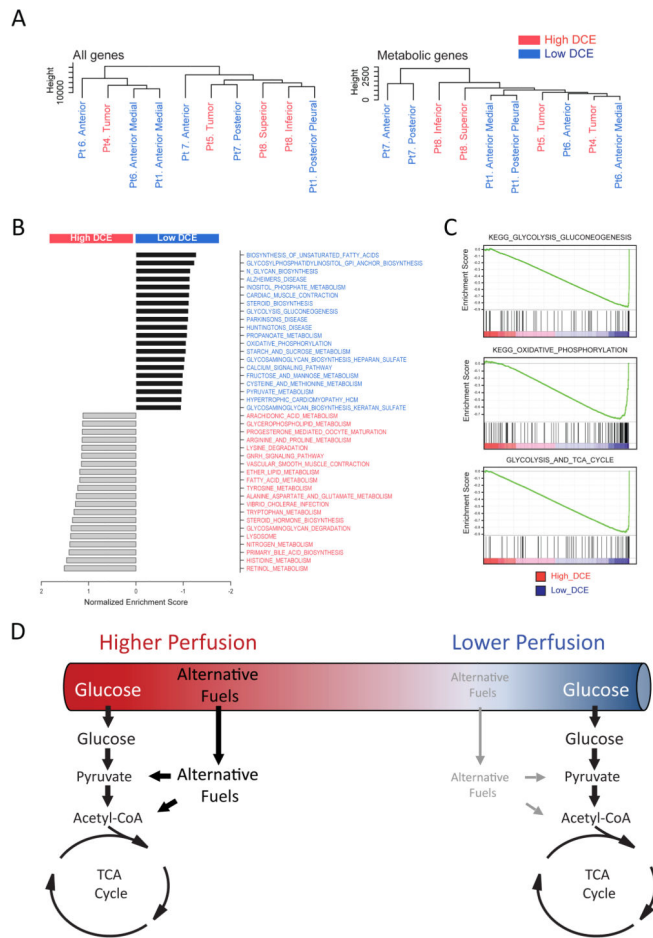
Figure 6. Gene expression signatures in tumors with high and low DCE signal

(A) Unsupervised clustering of RNA-Seq data from tumor fragments. Data included quantitation of all detected transcripts (left) or a subset of transcripts from 2,756 genes involved in metabolism.

(B) Results of GSEA using transcripts from metabolic genes. The 20 most enriched gene sets are shown for the high and low DCE groups.

(C) GSEA plots for three gene sets enriched in low DCE tumors.

(D) Proposed model for utilization of alternative fuels in NSCLC tumors with regional differences in perfusion.

Table 1

Clinical and pathological data from 9 NSCLC patients.

Pt.	Age	Sex	Smoking	Size	Histology	TNM stage	Grade	% Stroma	MVD	MIB-1	EGFR	KRAS	SUVmax
1	59	F	20	22.2	ADC (solid)	pT2aN0MX	G3	20	82	38	ND	G12C	10.2
2	74	F	45	1.6	ADC (ac)	pT1apN0MX	G1	50	180	17	ND	Q61H	NA
3	55	F	10	4.9	LCNEC	pT1bpN0pMX	G4	NA	NA	80	ND	ND	8.9
4	73	F	0	5.4	ADC (pap)	pT2aN0MX	G2	40	164	6	N771GY	ND	4.7
5	63	M	0	10.1	ADC (ac)	pT2aN0MX	G2	40	167	4	L858R	ND	5.1
6	81	M	120	15.5	ADC (pap)	pT2aN0MX	G2	20	215	19	L858R	ND	32
7	82	M	30	10.2	SQCC	cT1bN0M0	G3	20	142	25	ND	ND	8.3
8	66	F	0	16.1	ADC (ac/pap)	pT2aNpN1MX	G2	30	214	5	L858R	ND	13.3
9	43	M	0	3.8	ADC (mixed)	pt1bN0MX	G2	20	254	6	ND	ND	2.5

Smoking reflects smoking history in pack-years (average packs/day x years smoking). Tumor size is in cm^3 measured by T2 MRI. Key for histology: ADC, Adenocarcinoma; ac, acinar; pap, papillary; LCNEC, large cell neuroendocrine carcinoma; SQCC, squamous cell carcinoma. Key for TNM staging: T1a, greatest dimension 2cm; T1b, greatest dimension >2cm but 3cm; T2a, greatest dimension >3cm but 5cm; N0, regional node metastases absent; N1, ipsilateral peribronchial and/or ipsilateral hilar lymph nodes metastases present; MX, distant metastasis unknown; M0, distant metastases absent. Key for tumor grade: G1, well differentiated; G2, moderately differentiated. G3, poorly differentiated; G4, undifferentiated. % stroma is from a semiquantitative assessment of the fraction of area occupied by non-tumor cells. Microvessel density (MVD) is reported as number of vessels*10^{-6}/μm^2. Vessels were detected by CD31 IHC. MIB-1 is the fraction of cells with nuclear Ki67 staining. ND, no mutations detected. NA, tissue or images not available.